energies

MDPI

Article

Two Dimensional Thermal-Hydraulic Analysis for a Packed Bed Regenerator Used in a Reheating Furnace

Chien-Nan Lin [1], Jiin-Yuh Jang [2,*] and Yi-Shiun Lai [2]

[1] Department of Mechanical Engineering, Far East University, Tainan 74448, Taiwan; lincn@cc.feu.edu.tw
[2] Department of Mechanical Engineering, National Cheng-Kung University, Tainan 70101, Taiwan; n16034302@mail.ncku.edu.tw
* Correspondence: jangjim@mail.ncku.edu.tw; Tel.: +886-6-2088573

Academic Editor: Brian Agnew
Received: 22 August 2016; Accepted: 23 November 2016; Published: 25 November 2016

Abstract: Packed bed is widely used for different industries and technologies, such as heat exchangers, heat recovery, thermal energy storage and chemical reactors. In modern steel industry, packed bed regenerator is widely utilized in the reheating furnace to increase the furnace efficiency. This study established a two dimensional numerical model to simulate a packed bed used in regenerative furnaces. The physical properties of fluids and packed stuffing (such as density, thermal conductivity, and specific heat) are considered as functions of temperature to adapt the large temperature variation in operation. The transient temperature profiles of the flue gas, packed bed, and air during the heating and regeneration period are examined for various switching time (30, 60, 120, and 240 s). The results reveal that, during the heating period, the spanwise averaged heat transfer coefficient is decreased along the longitudinal downstream direction, while during the regeneration period, the opposite trend is true. Moreover, the regenerator thermal effectiveness is decreased by increasing the switching time.

Keywords: packed bed; heat exchanger; regenerator; reheating furnace

1. Introduction

In modern steel industry, a packed bed regenerator is widely utilized in the reheating furnace to increase the furnace efficiency. The regenerative furnace burners are mounted as couples at the opposite side of the furnace wall. The fuel and fresh air are injected into the combustion chamber from one burner and absorbed by another burner on the opposite side, as shown in Figure 1. The burner changes its function from being an injector to being an absorber, and vice versa, for every switching cycle. The burner switching function of the furnace includes three modes; the partial same-side-switching mode, the same-side-switching mode and the cross-switching mode. The packed bed restores the waste heat from the flue gas, and releases thermal energy to the fresh air before the combustion reaction. The regenerators use low heat-resistant, cheap material like alumina, and the medium used in the packed bed must be easily replaceable. During the furnace operation of furnace, about 80% of the exhaust gas flow via the spherical packed bed leaves the furnace, and the waste energy is stored in the packed bed. The remaining 20% of the exhaust gas flows directly to the furnace outlet. The thermal efficiency of the furnace is dominated by the temperature of inlet air, which is dependent on the burner setting and the packed bed design. Among the various structures, the spherical packed bed, with spherical diameter of 13 mm, is the superior with regard to achieving the goal of fuel reduction and green production.

In recent years, many studies have been concerned with air combustion technology at high temperatures in order to enhance thermal efficiency and reduce emission of NO_x. Ishii et al. [1,2] showed that 1579 K of preheat inlet air temperature can be obtained in a regenerative furnace.

Meanwhile, it produced low NO_x emissions and over 70% heating efficiency. Later, Stockwell et al. [3] examined the NO_x emission using a non-premixed combustion model in the regenerative furnace. Ou et al. [4] utilized transient simulation to discuss the effect of burner arrangement in a regenerative furnace. The results showed that the cross-switching combustion mode has the best performance among the three burner modes under consideration in their study, where the slabs could be heated to 1470 K. Coppage and London [5] investigated a counter flow regenerator by neglecting longitudinal heat conduction. They obtained a correlation for the thermal efficiency of a regenerator as a function of NTU, C*, C_r*, and (hA)*. Lambertson [6] derived an approximate solution for a counter flow regenerator at periodical steady state. His results showed that the influence of regeneration efficiency is insignificant for (hA)* ranging from 0.25 to 4. Nijemeisland et al. [7] numerically studied a packed bed by embedding 44 spheres in it and obtained a good agreement between the computational fluid dynamics (CFD) simulation and experiment. Guardo et al. [8] performed a numerical simulation for a packed bed with five *Reynolds-averaged Navier-Stokes* (RANS) turbulence models including standard κ-ε, standard-Allmaras, RNG κ-ε, Realizable κ-ε and standard κ-ω. They suggested that when the Reynold number coincides with the transition flow range, the standard-Allmaras model is recommended.

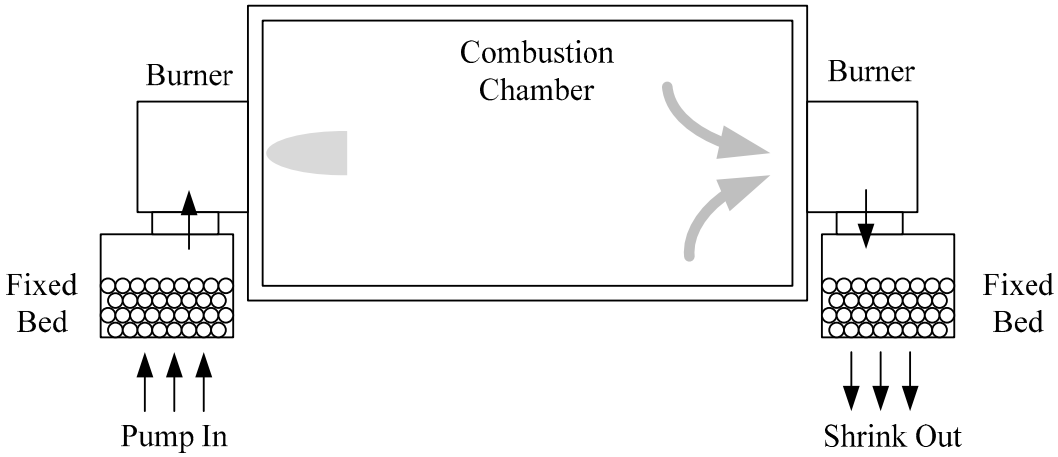

Figure 1. Schematic diagram of a regenerative furnace.

Jang and Chiu [9] simulated the cooling process of a sintered bed and proposed the correlations between the friction factor and the Nusselt number varied with the Reynold's number. Dong et al. [10] discussed the effect of switching time, length, and cell size for a honeycomb regenerator. They suggested a correlation for the thermal efficiency with normalized switching time and demonstrated the efficiency to be over 90%. Rafidi and Blasiak [11] used the number-transfer-unit (NTU) method to study the optimum regenerator length for a honeycomb regenerator. Rafidi [12] developed a mathematical model both used for the honeycomb and fixed bed types of heat regenerators used in HiTAC burning systems, and experimentally verified the temperature field. Their results revealed that in addition to the chemistry profiles uniformity, the temperature profiles were also more uniform in the case of HiTAC configurations; no high gradients of temperatures were found. Kang et al. [13] utilized the porous media module of the commercial software FLUENT to study the honeycomb regenerator of an oxy-fuel combustion furnace. The results were compared with experimental data. They showed that a longer honeycomb and shorter switching time result in greater thermal efficiency. Opitz et al. [14] simulated a packed-bed heat storage system using an ODE (ordinary differential equations) mathematic method and it is also applicable for a high Biot Number. Ortega et al. [15] experimentally and numerically studied the regeneration furnace by adopting slag as the medium of the packed bed. They found that the slag was stable at 1000 °C and could be sustained over 500 h, with thermal efficiency of about 95%. Schlipf et al. [16] used small grained material as the stuffing in a

packed bed, which was suited for low velocity at 550 °C of operating temperature. Cascetta et al. [17] used a local thermal non-equilibrium porous media model to simulate a two dimensional packed bed.

Since the switching time of the burners plays a key role in the heat storing and releasing process for a regenerative furnace, this has motivated the present investigation. The thermal efficiency of packed beds is affected by the heat transfer performance between the fluids and the packed stuffing. This study established a two dimensional numerical model to simulate the packed bed used in regenerative furnaces, owing to the three dimensional numerical simulation requires a huge computer time. The dynamic temperature profiles and the local heat transfer coefficient of the flue gas and packed stuffing are examined for various switching time (30, 60, 120, and 240 s).

2. Mathematical Formulation

Since the simulation of a three-dimensional transient packed bed model requires a huge amount of computational time, the three-dimensional model is simplified to a two-dimensional one, as shown in Figure 2. A packed bed is filled with aluminum oxide spheres (Al_2O_3) with diameter, D = 13 mm. For a unit cell, the flow length is 474 mm and its width is 10.2 mm. Table 1 shows the geometrical parameters used in this study.

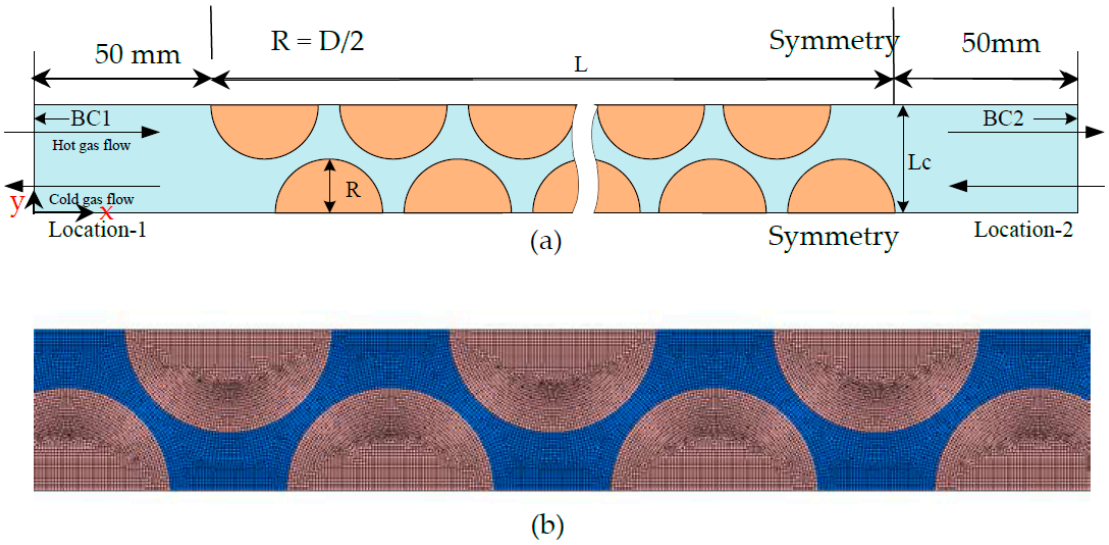

Figure 2. Schematic diagrams of (**a**) two-dimensional model and (**b**) computational grid system.

Table 1. Geometrical parameters and inlet velocities of two dimensional model.

Parameter	Value
Φ Porosity	0.36
D (mm) Diameter	13
Lc (mm)	10.2
Density of solid (kg/m^3)	3900
L (mm) Unit Length	474
Gas inlet velocity (m/s)	12.8
Air inlet velocity (m/s)	2.8

2.1. Governing Equations

The fluid is considered 2-D transient turbulent flow with variable properties, and the flow is assumed with no viscous dissipation. Equations for continuity, momentum (Reynolds averaged

Navier-Stokes equations), energy, turbulent kinetic energy, k, and the dissipation rate, ε, can be expressed in tensor form as follows:

$$\frac{\partial \rho}{\partial t} + \frac{\partial}{\partial x_i}(\rho u_i) = 0 \tag{1}$$

$$\frac{\partial}{\partial t}(\rho u_i) + \rho \frac{\partial}{\partial x_j}(u_i u_j) = -\frac{\partial p}{\partial x_i} + \frac{\partial}{\partial x_j}\left[\mu\left(\frac{\partial u_i}{\partial x_j} + \frac{\partial u_j}{\partial x_i} - \frac{2}{3}\frac{\partial u_i}{\partial x_i}\right)\right] + \frac{\partial}{\partial x_j}\left(-\rho\overline{u_i\prime u_j\prime}\right) \tag{2}$$

$$\frac{\partial}{\partial t}\rho c_p T + \frac{\partial}{\partial x_j}\rho c_p (u_i T) = \frac{\partial p}{\partial t} + u_j \frac{\partial p}{\partial x_j} + u_j\prime \frac{\partial p\prime}{\partial x_j} + \frac{\partial}{\partial x_j}\left(k\frac{\partial T}{\partial x_j} - \rho c_p \overline{u_j\prime T\prime}\right) \tag{3}$$

$$\frac{\partial}{\partial t}(\rho k) + \frac{\partial}{\partial x_i}(\rho k u_i) = \frac{\partial}{\partial x_j}\left[\left(\mu + \frac{\mu_t}{\sigma_k}\right)\frac{\partial k}{\partial x_j}\right] + \rho(P_r - \varepsilon) \tag{4}$$

$$\frac{\partial}{\partial t}(\rho \varepsilon) + \frac{\partial}{\partial x_i}(\rho \varepsilon u_i) = \frac{\partial}{\partial x_j}\left[\left(\mu + \frac{\mu_t}{\sigma_\varepsilon}\right)\frac{\partial \varepsilon}{\partial x_j}\right] + \rho\frac{\varepsilon}{k}(c_1 P_r - c_2 \varepsilon) \tag{5}$$

where

$$P_r = \frac{\mu_t}{\rho}\left[\left(\frac{\partial u_i}{\partial x_j} + \frac{\partial u_j}{\partial x_i}\right)^2 + 2\left(\frac{\partial u_i}{\partial x_j}\right)^2 - \frac{2}{3}(\nabla u_i)^2\right] - \frac{2}{3}\kappa\frac{\partial u_i}{\partial x_i} \tag{6}$$

$$\mu_t = \frac{\rho c_\mu \kappa^2}{\varepsilon} \tag{7}$$

In the above equations, u is the gas velocity, p is the gas pressure, T is the gas temperature, ρ is the gas density, x denotes the coordinate system, t denotes the time. μ is the gas viscosity. For κ-ε turbulent model, μ_t is the turbulent viscosity, $\sigma\kappa$ is the ratio of the momentum diffusion rate to the turbulent kinetic energy, P_r is the turbulent kinetic energy generation rate, $\sigma\varepsilon$ is the ratio of the momentum diffusion rate to the turbulent kinetic energy dissipation rate.

$$c_1 = 1.44,\ c_2 = 1.92,\ c_\mu = 0.09,\ \sigma_\kappa = 1.0,\ \sigma_\varepsilon = 1.3$$

The above empirical constants can be found from Launder and Spalding [18].

For the packed spheres (matrix), heat conduction is considered to be in the solid domain, where the transient heat conduction equation is

$$\rho c_s \frac{\partial T}{\partial t} = \frac{\partial}{\partial x_j}\left(k\frac{\partial T}{\partial x_j}\right) \tag{8}$$

In performing the computation, the variations of thermal conductivity and specific heat with temperature are shown in Figure 3, and they can be expressed as polynomials of temperature as follows:

$$k_s = 2.71 \times 10^{-11} T_s^4 - 1.36 \times 10^{-7} T_s^3 + 2.61 \times 10^{-4} T_s^2 - 0.229 T_s + 85.9 \tag{9}$$

$$c_s = -6.44 \times 10^{-10} T_s^4 + 2.96 \times 10^{-6} T_s^3 + 5.09 \times 10^{-3} T_s^2 + 4.0711 T_s - 49.908 \tag{10}$$

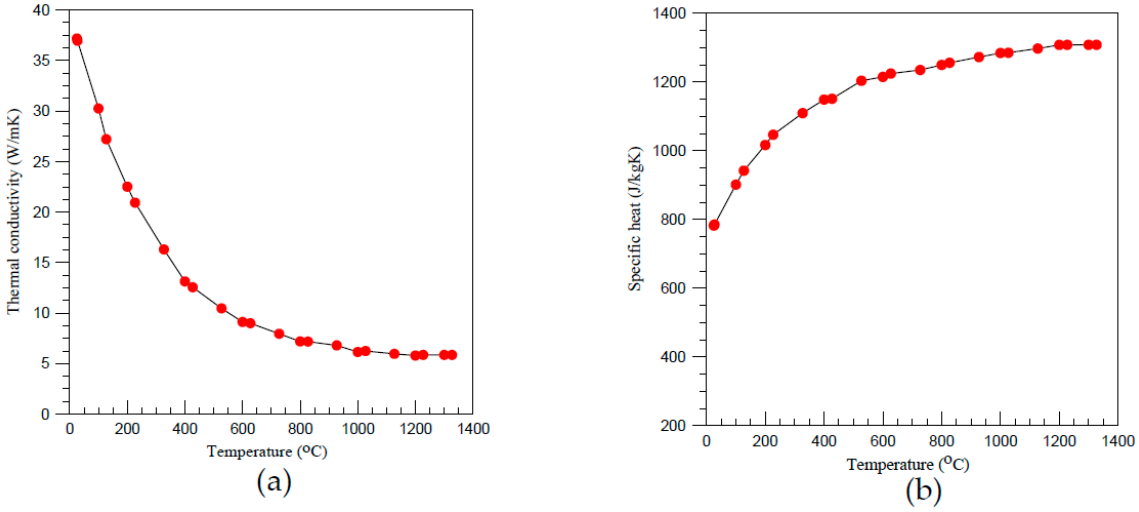

Figure 3. (**a**) Thermal conductivity and (**b**) specific heat of a packed sphere vs. temperature.

2.2. Initial and Boundary Conditions

An operation cycle is divided into the heating period and the regeneration period. During the heating period, the hot flue gas releases its energy to the packed bed (matrix) and the packed bed is heated in this period, while during the regeneration period, the packed bed rerelease its stored energy to the fresh air and the air is heated in this period. The flue gas is produced by the combustion of coal oven gas (COG). The mass fraction of flue gas is consisted of 12.46% of CO_2, 15.57% of H_2O, and 71.97% of N_2. During the heating period, the flue gas enters the packed bed at location 1 (x = 0) with velocity = 12.8 m/s at temperature of 1200 °C and leaves at location 2 (x = L), while during the regeneration period, the fresh air enters the packed bed at location 2 (x = L) with velocity =2.8 m/s at ambient temperate 27 °C and leaves at location 1 (x = 0). The fluid enters the packed bed with uniform velocity at the inlet, while the Neumann boundaries are assumed at the channel outlet.

$$\begin{array}{c} T_s\ (x,\ t_h = 0) = 27°\mathrm{C} \\ T_f\ (0,\ t_h) = 1200°\mathrm{C} \quad \text{for } 0 \le t_h \le \tau \end{array} \tag{11}$$

When the first heating period ends, the first regeneration period begins. The temperature of the packed sphere, $T_{s,x}$, is reserved as the initial condition of the regeneration period.

$$\begin{array}{c} T_s\ (x,\ t_r = \tau) = T_{s,x} \\ T_a\ (L,\ t_r) = 27°\mathrm{C} \quad \text{for} \quad \tau \le\ t_r \le 2\tau \end{array} \tag{12}$$

Similarly, the calculated temperature of the packed spheres at the end of regeneration period is reserved as the initial condition of the next heating period.

2.3. Heat Transfer Coefficient and Regenerator Temperature Effectiveness

The local heat transfer coefficient h is defined as:

$$h = \frac{q''}{T_w - T_b} \tag{13}$$

where q'' is the local heat flux. T_b is the local bulk mean temperature, which is s obtained by averaging the temperatures along with the spanwise direction y for a given x. T_w is the wall temperature of the packed spheres.

Since the gas temperature at the outlet is function of time, the average temperature for an operation cycle is described as

$$\overline{T_{out}} = \frac{1}{\tau}\int_0^{\tau} T_{out}(t)dt \tag{14}$$

The regenerator thermal effectiveness is defined as the ratio of actual heat transfer rate after an operating cycle to the thermo-dynamically limited maximum possible heat transfer rate:

$$\varepsilon = \frac{q}{q_{\max}} = \frac{C_h(T_{h,i} - \overline{T_{h,o}})}{C_{\min}(T_{h,i} - T_{c,i})} = \frac{C_c(\overline{T_{c,o}} - T_{c,i})}{C_{\min}(T_{h,i} - T_{c,i})} \tag{15}$$

where, C_h and C_c, represents the heat capacity rate of the hot flue gas and cold air, respectively. $C_{\min}$ is the minimum of C_h and C_c. In this study, the $C_{\min}$ is equal to C_c.

3. Numerical Method

In this study, the governing equations are solved numerically using a control volume based finite difference formulation, ANSYS-Fluent. The numerical methodology is briefly described here. Finite difference approximations are employed to discretize the transport equations on non-staggered grid mesh systems. A third-order upwind TVD (total variation diminishing) scheme is used to model the convective terms of governing equations. Second-order central difference schemes are used for the viscous and source terms. A pressure based predictor/multi- corrector solution procedure is employed to enhance velocity-pressure coupling and continuity-satisfied flow filed. In order to verify the accuracy of the present physical model, we had compared our numerical results with those of Rafidi and Blasiak [11] for a honeycomb regenerator, the numerical accuracy is within 5%.

A careful check for the grid-independence of the numerical solutions has been made to ensure the accuracy and validity of the numerical results. For this purpose, five grid systems, 50,000, 100,000, 150,000, 200,000 and 400,000 were tested. It was found that for switching time = 60 s, the relative errors in the thermal effectiveness for the solutions of 200,000 and 400,000 were less than 1%, as shown in Figure 4. Therefore, a grid system of 200,000 was typically adopted in this computational domain. The convergence criterion is satisfied when the residuals of all variables are less than 1.0×10^{-6}. Computations were performed on a 3.0 GHz Intel® Core™ 10 processor with 100 GB of memory and typical CPU times were 24 h to obtain the pseudo-steady solution.

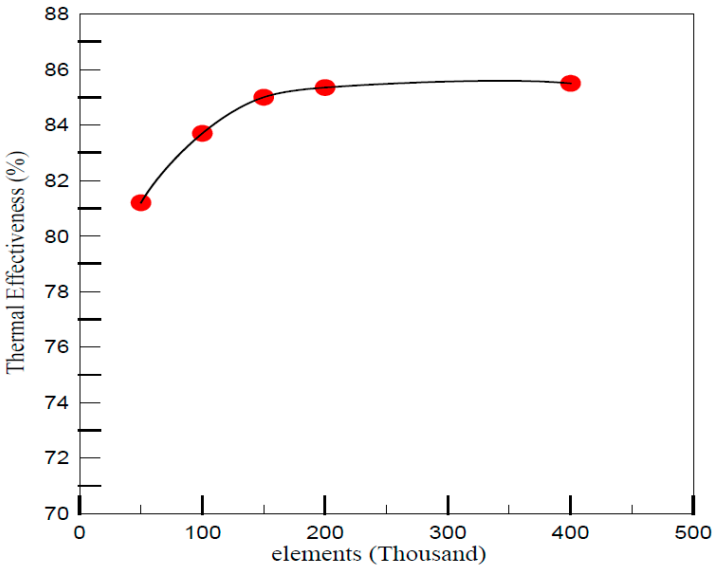

Figure 4. The thermal effectiveness vs. grid number for switching time = 60 s.

4. Result and Discussion

Figure 5 shows the streamline distribution for the heating and regeneration periods for switching time = 60 s. During the heating period, the flue gas releases its energy to the packed bed, this results in the flue gas temperature is decreased and its density is increased along the longitudinal downstream direction (x = 0 to L). Therefore, based on the conservation of of mass, it is seen from Figure 5a that the spanwise averaged velocty of flue gas is decreased from x = 0 to x = L. In constrast, during the regeneration period, the air temperature is increased and its density is decreased from x = L to 0. Thus, the spanwise averaged air velocity is increased from from x = L to 0, as shown in Figure 5b.

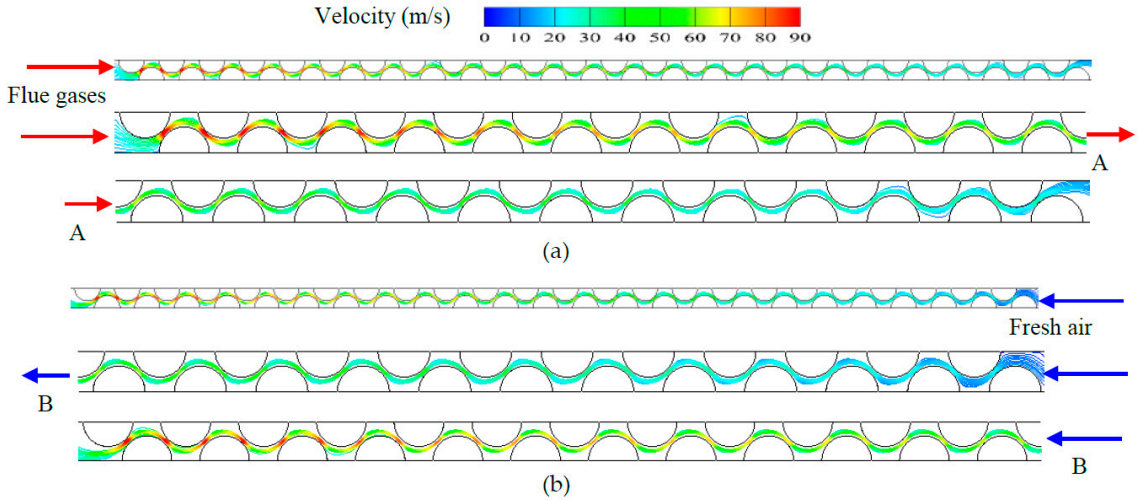

Figure 5. Streamline for (**a**) heating period; (**b**) regeneration period.

Figure 6a,b shows the transient temperature variation for 3 different time (0, 30 and 60 s for heating period, 63, 90 and 120 s for regeneration period) at the pseudo steady state operation cycle (0 to 120 s) during the heating (0 to 60 s) and regeneration period (60 to 120 s), respectively, for switch time = 60 s. During the first heating period, the flue gas enters the packed bed at location 1 (x = 0) and releases its thermal energy to heat the packed spheres. The temperature of the packed spheres is increased with time, while it is decreased along with the longidudinal downstream direction. During the regeneration period, the cold fresh air flows into the packed bed at location 2 (x = L) and absorbs the thermal energy stored in the packed spheres. Thus, the air temperature is significantly increased to its outlet (Location 1, x = 0).

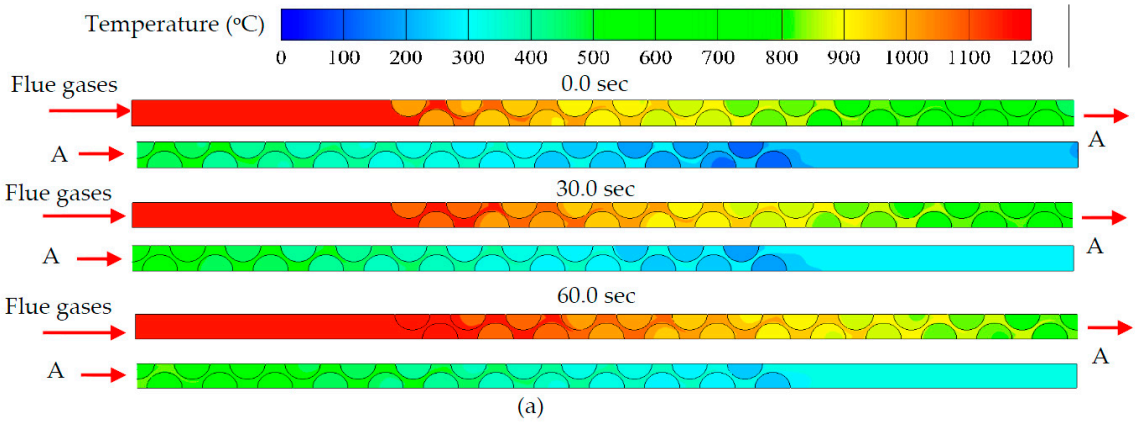

Figure 6. *Cont.*

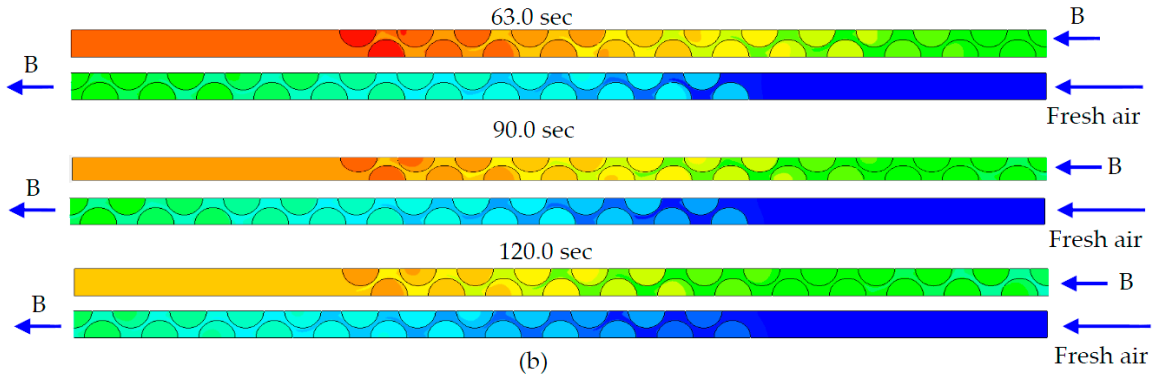

Figure 6. Temperature contour for 3 different time at pseudo-steady state during (**a**) heating period; and (**b**) regeneration period for switching time = 60 s.

Figure 7 displayed the spanwise averaged heat transfer coefficient along the length of packed bed. The spanwise averaged hat transfer is calculated by averaging the local heat transfer coefficients along with the spanwise direction y for a given x. Since the spanwise averaged velocty of flue gas is decreased from x = 0 to x = L, this results in the spanwise averaged heat transfer coefficient is decreased along the longitudinal downstream direction, as shown in Figure 7a. In constrast, during the regeneration period, the air velocity is increased along the longitudinal downstream direction (x = L to 0), this results in the spanwise averaged heat transfer coefficient is increased along the longitudinal downstream direction, as shown in Figure 7b.

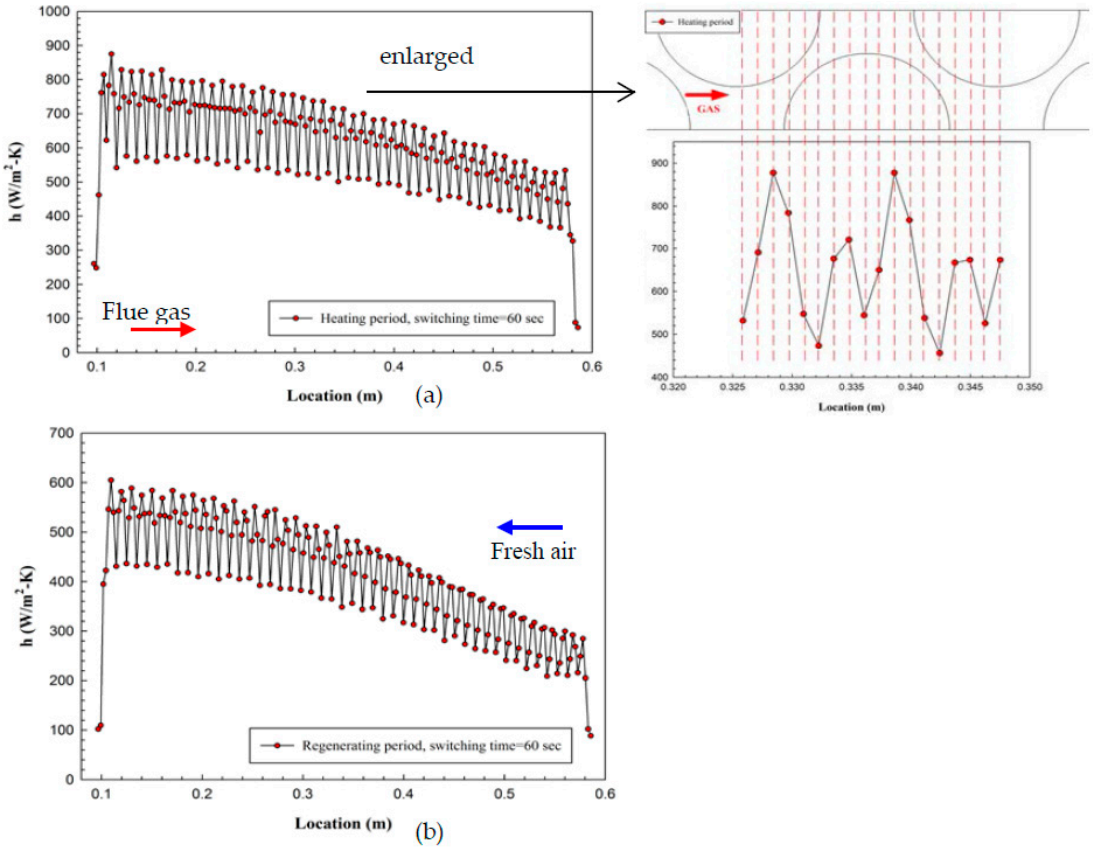

Figure 7. The variations of the spanwise averaged heat transfer coefficient vs. axial position during (**a**) heating period and (**b**) regeneration periods for switching time = 60 s.

Figure 8a–c shows the temperature variations at location 1 (x = 0) and 2 (x = L) with time for a time period of 60 min for switching time 30, 60, and 120 s, respectively. During the heating period, since the flue gas enters at location 1 (x = 0), and leaves at location 2 (x = L), the temperature of location 1 (x = 0) remain a constant temperature, 1200 °C, and the matrix temperature at location 2 (x = L) is rising with time. While switching to the regeneration period, the air enters at location 2 (x = L) with temperature of 27 °C and obtains thermal energy from the matrix. This results in a suddenly drop of temperature at location 2 (x = L) and also the matrix temperature is decreeing with time at location 1 (x = 0). One can observe that, a shorter switching time requires more operation cycles to achieve the pseudo-steady state. It is also found that, with increasing switching time, the flue outlet temperature is increased, while the air outlet temperature is decreased. This results in the decrease of the regenerator temperature effectiveness for larger switching time.

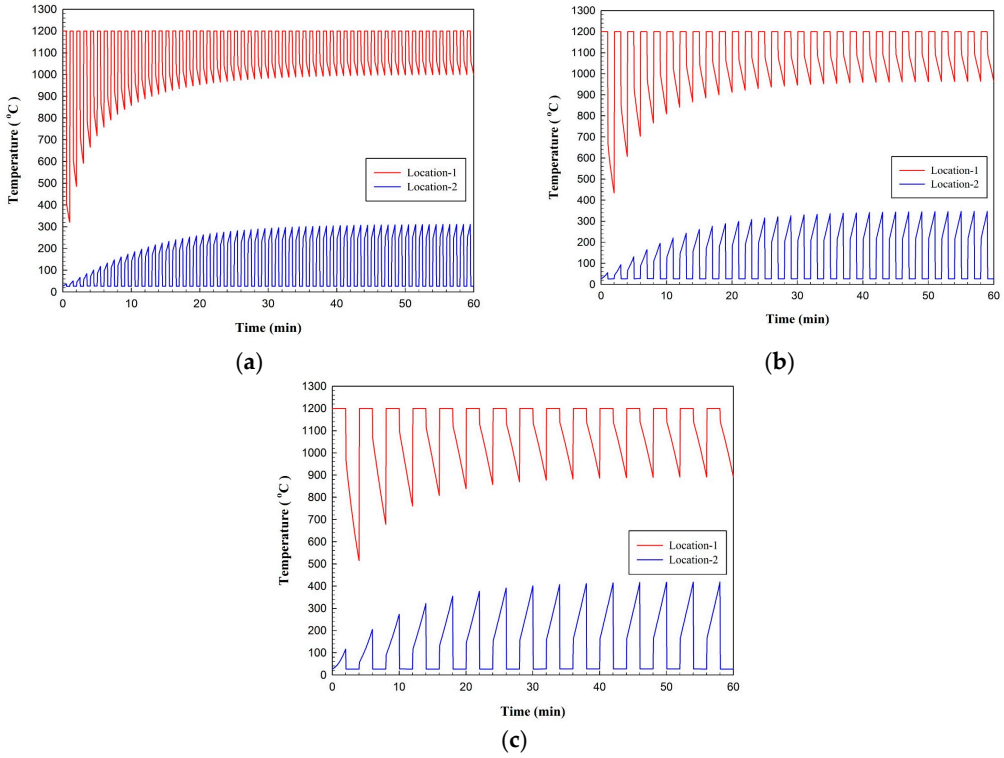

Figure 8. The temperature variations at location 1 (x = 0) and 2 (x = L) with time for a time period of 60 min for switching time (**a**) 30 s; (**b**) 60 s; and (**c**) 120 s.

Figure 9 shows the corresponding variation of spanwise averaged temperatures of flue gas, packed bed (matrix) and air along the longitudinal direction x for switching time = 60 s. The solid lines denote the temperatures for the flue and air, while the dashed lines denote the matrix temperature. During the heating period, since the matrix gradually absorbs thermal energy from the flue gas, the matrix temperature is increased with time. This results in, as the time is increased, the temperature difference between the flue gas and matrix is decreased and the flue gas outlet temperature is increased. While during the regeneration period, since the matrix gradually releases thermal energy to the fresh air, the matrix temperature is decreased with time. It is observed that the temperature variation is not so smooth at the end location due to the switching process at time beginning of each cycle. In contrast, the temperature variation is smoother between the end locations than the entrance regions. Although the variation of local heat transfer coefficient is changing rapidly as shown in Figure 7, the gas velocity is large enough to smooth the abrupt change of heat transfer rate. Note that the flue gas enters the packed bed at location 1 (x = 0) with velocity =12.8 m/s, while during the regeneration period, the fresh air enters the packed bed at location 2 (x = L) with velocity = 2.8 m/s. These two velocities

were determined from a packed bed regenerator used in the reheating furnace a real steel plant in Taiwan.

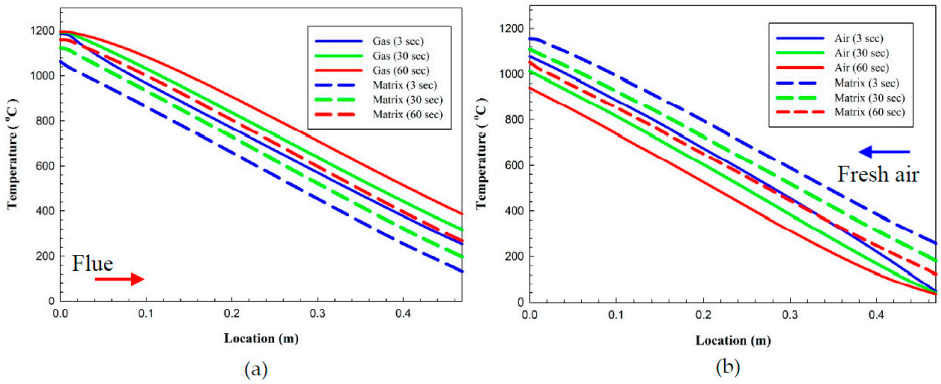

Figure 9. Temperature variation with locations for 3 different time at pseudo-steady state during (**a**) heating period; and (**b**) regeneration period for switching time = 60 s.

Figure 10 illustrates the variation of regenerator thermal effectiveness with switching time. It is seen that he regenerator thermal effectiveness is decreased with increasing the switching time. It is 85.6%, 85.4%, 84.7%, and 82.2% for the switching time of 30, 60, 120, and 240 s, respectively. The conventional furnace uses the recuperator to preheat the air, which can only increase the air temperature up to 450 °C. However, by using the packed bed regenerator with thermal effectiveness 85.4%, the air temperature can be preheated up to 1000 °C. This corresponds to 14% COG energy saving. In contrast, an 82.2% thermal effectiveness, the air temperature can be preheated up to 930 °C, and 13% COG energy saving was obtained. Take a conventional furnace with 60 m in length for example, 44 pieces of slabs with dimensions of 10 m × 1.25 m × 0.25 m in the furnace simultaneously, the resident time is about 200 min for each slab. The COG consumption is about 2.27 kg/s, it is 0.318 kg/s saving for the reheating furnace with 85.4% thermal effectiveness. A shorter switching time yields effective heat transfer between fluids and spheres due to frequent interchanged heat. Conversely, a longer switching time incurs a decreasing temperature difference between the fluids and the packed spheres as the operation progressing for every cycle, which results in decreasing thermal effectiveness. However, shorter switching time indicates rapid temperature changes for the packed sphere and results in a decrease in the lifetime of the packed sphere. Accordingly, the optimum switching time used in the regeneration furnace should take the economical parameter into account.

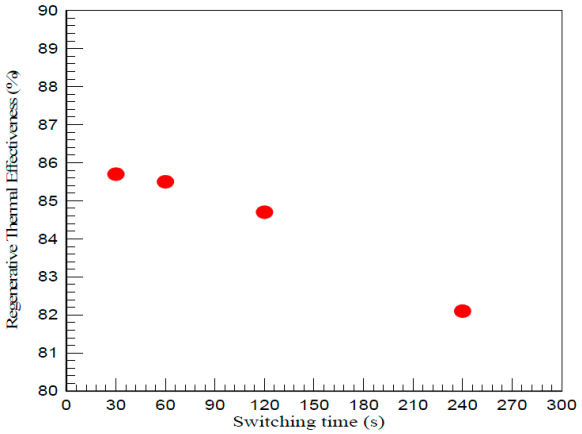

Figure 10. The variations of regenerative thermal effectiveness vs. switching time.

5. Conclusions

Two dimensional transient turbulent fluid flow and heat transfer in a packed sphere bed used in a regenerator furnace are studied numerically. Based on the results, the following important conclusions are summarized as follows:

1. During the heating period, the average flue gas velocity is decreased along the longitudinal downstream direction (x = 0 to L). This results in the spanwise averaged heat transfer coefficient is decreased along the longitudinal downstream direction, while during the regeneration period (x = L to 0), the opposite trend is true.
2. A shorter switching time requires more operation cycles to achieve the pseudo-steady state. With increasing switching time, the flue outlet temperature is increased, while the air outlet temperature is decreased. This results in the decrease of the regenerator thermal effectiveness for larger switching time.

Acknowledgments: This research was financially supported by the Ministry of Science and Technology, Taiwan, under contracts MOST 104-2622-8-006-001.

Author Contributions: All authors contributed to this work. Chien-Nan Lin performed numerical modeling and data reduction. Jiin-Yuh Jang performed theoretical model. Yi-Shiun Lai executed the numerical work and data reduction.

Conflicts of Interest: The authors declare no conflict of interest.

Nomenclature

C	heat capacity rate ($W \cdot K^{-1}$)
c_s	specific heat ($kJ \cdot kg^{-1} \cdot K^{-1}$)
D	diameter (mm)
h	convection heat transfer coefficient ($W \cdot m^{-2} \cdot K^{-1}$)
k	thermal conductivity ($W \cdot m^{-1} \cdot K^{-1}$)
L	flow length (mm)
L_c	flow channel width (mm)
Nu	Nusselt number
n	computational period number
p	Pressure (pa)
Pr	Prandtl number
Re	Reynold number
r	radial direction of packed sphere
T	temperature (°C)
t	time (s)
u_i	velocity component ($m \cdot s^{-1}$)
x_i	coordinate
α	thermal diffusivity ($m^2 \cdot s^{-1}$)
ε	thermal effectiveness
ρ	density ($kg \cdot m^{-3}$)
Φ	porosity
τ	switching time (s)
μ	viscosity ($N \cdot s \cdot m^{-2}$)

Subscript

a	air
f	flue gas

h	heating period
c	cold flow fluid
i	inlet
min	minimum
max	maximum
o	outlet
r	regeneration period
s	packed sphere

References

1. Ishii, T.; Zhang, C.; Suglyama, S. Numerical simulations of highly preheated air combustion in an industrial furnace. *Trans. ASME* **1998**, *120*, 276–284. [CrossRef]
2. Ishii, T.; Zhang, C.; Suglyama, S. Effects of NO Models on the prediction of NO formation in a regenerative furnace. *Trans. ASME* **2000**, *122*, 943–957. [CrossRef]
3. Stockwell, N.; Zhang, C.; Ishii, T.; Hino, Y. Numerical simulations of turbulent non-premixed combustion in a regenerative furnace. *ISIJ Int.* **2001**, *41*, 1272–1281. [CrossRef]
4. Ou, J.P.; Ma, A.C.; Zhan, S.H.; Zhou, J.M.; Xiao, Z.Q. Dynamic simulation on effect of flame arrangement on thermal process of regenerative reheating furnace. *J. Cent. South Univ. Technol.* **2007**, *14*, 243–247. [CrossRef]
5. Coppage, J.E.; London, A.L. The periodic-flow regenerator—A summary design theory. *Trans. ASME* **1953**, *75*, 779–787.
6. Lamberston, T.J. Performance factors of a periodic-flow heat exchanger. *Trans. ASME* **1958**, *80*, 586–592.
7. Nijemeisland, M.; Dixon, A.G. Comparison of CFD simulations to experiment for convective heat transfer in a gas-solid packed bed. *Chem. Eng. J.* **2001**, *82*, 231–246. [CrossRef]
8. Guardo, A.; Coussirat, M.; Larrayoz, M.A.; Recasens, F.; Egusquiza, E. Influence of the turbulence model in CFD modeling of wall-to-fluid heat transfer in packed beds. *Chem. Eng. Sci.* **2005**, *60*, 1733–1742. [CrossRef]
9. Jang, J.Y.; Chiu, Y.W. 3-D Transient conjugated heat transfer and fluid flow analysis for the cooling process of sintered bed. *Appl. Therm. Eng.* **2009**, *29*, 2895–2903. [CrossRef]
10. Noh, D.S.; Hong, S.K.; Ryou, H.S.; Lee, S.H. An experimental and numerical study on thermal performance of a regenerator system with ceramic honeycomb. *KSME Int. J.* **2001**, *15*, 357–365. [CrossRef]
11. Rafidi, N.; Blasiak, W. Thermal performance analysis on a two composite material honeycomb heat regenerators used for HiTAC burners. *Appl. Therm. Eng.* **2005**, *25*, 2966–2982. [CrossRef]
12. Rafidi, N. Thermodynamic Aspects and Heat Transfer Characteristics of HiTAC Furnaces with Regenerators. Ph.D. Thesis, Royal Institute of Technology, Stockholm, Sweden, 2005.
13. Kang, K.; Hong, S.K.; Noh, D.S.; Ryou, H.S. Heat transfer characteristics of a ceramic honeycomb regenerator for an oxy-fuel combustion furnace. *Appl. Therm. Eng.* **2014**, *70*, 494–500. [CrossRef]
14. Opitz, F.; Treffinger, P. Packed bed thermal energy storage model-Generalized approach and experimental validation. *Appl. Therm. Eng.* **2014**, *73*, 245–252. [CrossRef]
15. Ortega, I.; Faik, A.; Gil, A.; Rodriguez-Asequinolaza, J.; D'Aguanno, B. Thermo-physical properties of a steel-making by-product to be used as thermal energy storage material in a packed-bed system. *Energy Procedia* **2015**, *69*, 968–977. [CrossRef]
16. Schlipf, D.; Schicktanz, P.; Maier, H.; Schneider, G. Using sand and other small grained. *Energy Procedia* **2015**, *69*, 1029–1038. [CrossRef]
17. Cascetta, M.; Cau, G.; Puddu, P.; Serra, F. A comparison between CFD simulation and experimental investigation of a packed-bed thermal energy storage system. *Appl. Therm. Eng.* **2016**, *98*, 1263–1272. [CrossRef]
18. Launder, B.E.; Spalding, D.B. *Mathematics Models of Turbulence*; Academic Press: London, UK, 1972; Chapter 5.